Journal Pre-proof

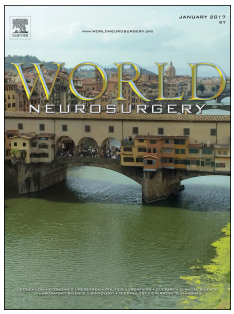

Differentiating non enhancing grade II gliomas from grade III gliomas using diffusion tensor imaging and dynamic susceptibility contrast MRI

Hatham Alkanhal, Kumar Das, Nitika Rathi, Khaja Syed, Harish Poptani

PII: S1878-8750(20)32346-9

DOI: https://doi.org/10.1016/j.wneu.2020.10.144

Reference: WNEU 16242

To appear in: *World Neurosurgery*

Received Date: 22 June 2020

Revised Date: 25 October 2020

Accepted Date: 26 October 2020

Please cite this article as: Alkanhal H, Das K, Rathi N, Syed K, Poptani H, Differentiating non enhancing grade II gliomas from grade III gliomas using diffusion tensor imaging and dynamic susceptibility contrast MRI, *World Neurosurgery* (2020), doi: https://doi.org/10.1016/j.wneu.2020.10.144.

I, Harish Poptani, certify that this manuscript is a unique submission and is not being considered for publication, in part or in full, with any other source in any medium.

I would also like to certify that all authors have made significant contribution to the design, acquisition and analysis of data as well as writing of this manuscript

With regards

Harish Poptani

Title: Differentiating non enhancing grade II gliomas from grade III gliomas using diffusion tensor imaging and dynamic susceptibility contrast MRI

Short Title: DTI and DSC in non-enhancing gliomas.

Type of manuscript – Research article

Authors: Hatham Alkanhal[1], Kumar Das[2], Nitika Rathi[3], Khaja Syed[3], Harish Poptani[1]

[1] Centre for Preclinical Imaging, University of Liverpool, Liverpool, United Kingdom.

[2] Department of Neuroradiology, Walton Centre NHS trust, Liverpool, United Kingdom.

[3] Department of pathology, Walton Centre NHS trust, Liverpool, United Kingdom.

*Corresponding author:

Professor Harish Poptani

Centre for Preclinical Imaging,

Nuffield Wing, Sherrington Building

Crown Street, Liverpool L69 3BX

United Kingdom

Phone: +44 151 794 5444

E-mail address: Harish.Poptani@liverpool.ac.uk

Keywords: non-enhancing gliomas; diffusion tensor imaging; dynamic susceptibility contrast; astrocytomas; oligodendrogliomas

Differentiating non enhancing grade II gliomas from grade III gliomas using diffusion tensor imaging and dynamic susceptibility contrast MRI

Abstract:

Background: Contrast enhancement in a brain tumour MRI is typically indicative of a high-grade glioma. However, a significant proportion of non-enhancing gliomas can either be grade II (GII) or grade III (GIII). Whilst gross total resection remains the primary goal, imaging biomarkers may guide management where surgery is not possible, especially for non-enhancing gliomas. The utility of diffusion tensor imaging (DTI) and dynamic susceptibility contrast (DSC) MRI was evaluated in differentiating non-enhancing gliomas.

Methods: Retrospective analysis was performed on MRI data from 72 non-enhancing gliomas, including GII (n = 49) and GIII (n=23) gliomas. DTI and DSC data were used to generate fractional anisotropy, mean diffusivity, axial diffusivity and radial diffusivity as well as cerebral blood volume, cerebral blood flow and mean transit time (MTT) maps. Univariate and multi-variate logistic regression along with area under the curves (AUC) analyses were used to measure the sensitivity and specificity of imaging parameters. A sub-analysis was performed to evaluate the utility of imaging parameters in differentiating between different histological groups.

Results: Logistic regression analysis indicated that tumour volume and relative MTT could differentiate between GII and GIII non-enhancing gliomas. At a cut-off value of 0.33, this combination provided an AUC of 0.71, 70.6% sensitivity and 64.3% specificity. The logistic regression analyses demonstrated much higher sensitivity and specificity in the differentiation of astrocytomas from oligodendrogliomas or identification of grades within these histological subtypes.

Conclusion: DTI and DSC imaging can aid in the differentiation of non-enhancing GII and GIII gliomas, and between histological subtypes.

Introduction:

Gliomas are the most common primary brain tumours and are generally classified as low- or high-grade. Pre-surgical diagnosis of a glioma is typically performed using magnetic resonance imaging (MRI). On post-contrast enhanced images, high-grade gliomas (HGG) generally appear hyperintense due to breakdown of blood-brain barrier, while low-grade gliomas (LGG) typically do not [1]. However, several exceptions to this rule exist, as around 14–45% of non-enhancing gliomas turn out to be high-grade and, conversely, some LGG exhibit contrast enhancement [2, 3]. Therefore, accurately grading non-enhancing gliomas is necessary for planning optimal treatment strategies [4,5]. Conventional contrast enhanced MRI may not be able to differentiate between the various grades. Although the World Health Organisation (WHO) has revised glioma classification in 2016 laying more emphasis on molecular markers than grading based on morphological features alone, histopathological diagnoses and clinical management is still prevalently reported using the I-IV grading scale. While surgical resection is often the first line of treatment for most gliomas, optimal treatment strategy for patients, including LGG, is influenced by several factors including molecular characterization, location and clinical symptoms [6,7]. The ideal treatment for LGG is still evolving and varies between different institutions. Surgical resection is performed to remove as much of the tumour as safely possible as well as for a histological and molecular diagnosis. If surgical resection is not appropriate, biopsy is often considered to obtain histological and molecular diagnosis. Depending on the molecular subtype of GII glioma, surgery may be followed by radiotherapy and chemotherapy. In GIII glioma, on the other hand, surgical resection is typically followed by sequential radiotherapy followed by chemotherapy, guided by Karnofsky performance status and tumour molecular markers. In the patient group where surgery is not possible or patient declines surgery, MRI features (GII versus GIII) may guide relative frequency of the imaging surveillance, site of potential biopsy, and further management.

Although final diagnosis is determined using surgical samples, presurgical diagnosis using MRI can aid in proper treatment planning. The limitations of conventional imaging for accurate grading, especially in non-enhancing gliomas, has led to the evaluation of advanced MRI methods, such as diffusion tensor imaging (DTI) and dynamic susceptibility contrast perfusion-weighted imaging (DSC-PWI) in these cases [8].

DTI has been used to aid in the diagnosis and surgical planning of brain tumours, with mean diffusivity (MD) or the apparent diffusion coefficient (ADC) the most common DTI parameters used. Fan et al. (2006) reported a significant difference in the mean ADC of non-enhancing LGG and HGG [9]. However, mixed results have been reported with fractional anisotropy (FA), another commonly used DTI parameter. One study reported no difference between LGG and Anaplastic Astrocytomas [10]. Similarly another study, comparing non-enhancing regions of HGGs with non-enhancing LGGs, did not observe any significant difference in FA values [11]. However, some studies have suggested a positive relationship between the FA values of LGG and HGG [12, 13].

DSC- perfusion weighted imaging (DSC-PWI) is a commonly used MRI technique for grading gliomas and predicting survival [14]. It is used to estimate three key parameters related to tumour hemodynamics, namely cerebral blood volume (CBV), cerebral blood flow (CBF) and mean time transit (MTT) [15, 16]. CBV represents the degree of vascular volume in tumours [17], an important parameter in determining the biological aggressiveness and grading of gliomas [17]. Sahin et al. (2013) suggested DSC-PWI as a fundamental tool for evaluating non-enhancing gliomas [18]. Some studies reported that the relative CBV (rCBV) ratio of non-enhancing HGG was significantly higher than non-enhancing LGG [19, 20]. Another study reported that maximum rCBV ratios were higher in GIII Astrocytomas than GI & II Astrocytomas [4].

Although DTI and DSC have been widely used in grading gliomas, most published studies are based on evaluating enhancing tumours, or compared enhancing tumours to non-enhancing tumours. In addition, many studies suffer from a limited patient cohort or have grouped GI & GII (LGG) and GIII & GIV (HGG). While this strategy has some clinical relevance, differentiation between non-enhancing GII and GIII glioma has proved challenging [3, 21, 22]. Accurate diagnosis of non-enhancing GII from GIII gliomas as highly desirable as it helps in proper treatment planning, especially in cases of diffused tumour boundaries, risks of comorbidities or when the tumour location is such that it cannot be resected.

Thus, the purpose of this study was to evaluate whether conventional MRI, in combination with DTI and DSC-PWI, can differentiate between non-enhancing GII and GIII gliomas. Since Astrocytomas and Oligodendrogliomas are distinct histological sub-types with different prognoses and responses to chemotherapy, a sub-analysis was also performed to differentiate between non-enhancing Astrocytomas and Oligodendrogliomas. Typically, the differentiation

between oligodendroglioma and astrocytoma is based on molecular markers. As per the revised WHO guidelines, oligodendrogliomas are categorized based on classical morphology as well as presence of IDH gene mutation and 1p/19q codeletion. Astrocytomas, on the other hand are represented by an abundance of astrocytic cells and IDH mutation, but without 1p/19q codeletion.

Methods:

Patient population:

This retrospective study was approved by the local research ethics committee at Liverpool University and the Walton Centre, Liverpool. As pseudo anonymized pre-existing MRI data was used, specific patient consent was waived. The data comprised of pre-existing MR images of patients with non-enhancing WHO grade II and grade III gliomas, acquired between January 2006 and January 2017. All patients (N= 72, 40 men and 32 women; mean age, 40 years; age range, 24–67 years) had received their initial imaging based diagnosis from neuroradiologists, which was subsequently confirmed by histology of the biopsy/surgical samples. Based on histological features and 1p19q status, patients were classified as (GII or GIII) astrocytoma or oligodendroglioma as shown in Table 1. Reclassification of any previous diagnosis of "mixed grade" or oligo-astrocytomas was performed using the revised 2016 WHO central nervous system (CNS) tumour classification. All patients had conventional sequential T1 weighted, T2 weighted and post contrast T1 volumetric sequences. DSC-PWI data was available from all 72 patients while DTI data was only available from 43 patients as the saved dicom DTI data files from these patients did not contain the information about the b values and b vectors.

Data acquisition parameters:

The MR data was acquired on clinical 3T scanners operating either using the General Electric (MR 750), Philips (Achieva) or Siemens (Trio) consoles. Conventional imaging included T1 weighted, T2 weighted and T1 weighted post contrast images, followed by DTI and DSC imaging. FLAIR images were only available infrequently for some patients and hence were not used in the analysis. For DSC imaging, rapid images of the brain were acquired using a T2* weighted sequence starting 10 s before intravenous injection of a standard dose of the gadolinium-based contrast agent (0.1 mmol/kg body weight) at a rate of 4 mL/s, followed by a 20 mL continuous saline flush, and continued for a total acquisition time of 90 s. Typical

sequence and data acquisition parameters for each of the scanners used are shown in supplementary Table 1.

Image processing:

The DSC data post-processing was performed using nordicICE (Nordic Neuro Lab AS, Bergen, Norway) software. The effects of contrast agent leakage were corrected using a residue function-based method [23]. To reduce motion artefacts, motion correction was performed by rigid co-registration method in the nordicICE software. Automatic identification of the arterial input function (AIF) was used to select the AIF [24] and standard singular value decomposition (sSVD) was used for the deconvolution process [25] for the computation of parametric maps including CBV, CBF and MTT.

The DTI data post-processing was performed using the Functional Magnetic Resonance Imaging of Brain (FMRIB) software library (FSL). Motion, eddy current and susceptibility artefacts were corrected [26] using FSL, and parametric maps of FA, MD, axial diffusivity (AD) and radial diffusivity (RD) were generated.

To account for the differences in image resolution and slice thickness from the three scanners as well as between different sequences, axial T2 weighted images were initially co-registered and resampled to the resolution of the DTI and DSC images so that all images had the same resolution as shown in Figure 1.

A volume of interest (VOI) was generated using the manual segmentation tool in Amira (Thermo Fischer Scientific, France) software to segment the tumour on re-sampled T2 weighted images covering the entire T2 weighted signal abnormality on each slice. The segmented tumour volume was confirmed by a neuroradiologist with over 17 years experience. The area from all slices was then summed to compute the VOI (Figure 1). The same VOIs were then used for DTI and DSC maps. To account for the variability in acquisition parameters from different scanners and between patients, tumour values were normalized to the contralateral normal brain. Three VOIs were typically generated from each patient including the tumour, a contralateral VOI, similar in volume to the tumour VOI, and a contralateral white matter VOI to compute the normalized DSC parameters (rMTT, rCBF and rCBV). To mitigate for sampling bias and evaluate viable tumour regions, the 90^{th} and 10^{th} percentiles of the rCBV and MD values were measured within the entire tumour VOI, and reported as $rCBV_{max}$ and MD_{min}.

Statistical analysis:

The data were analysed using Statistical Program for Social Science (SPSS) version 24 (IBM, UK). Quantitative data were represented as median ± standard deviation (SD). Following histogram analysis, the data was found to be non-normally distributed, and hence a non-parametric Mann-Whitney U test was used to analyse tumour volume, normalized T2 (nT2) signal intensity, DSC and DTI parameters. Comparisons were made between GII versus GIII gliomas, astrocytomas versus oligodendrogliomas, GII astrocytoma versus GII oligodendroglioma, and GII astrocytoma versus GIII anaplastic astrocytoma. A p-value of < 0.05 was considered significant for the univariate analysis. A logistic regression analysis was performed using a backward methodology to determine the best combination of parameters to differentiate between groups. A leave-one-out cross validation (LOOCV) analysis was used to validate the sensitivity and specificity of the combined parameters. This method employs a leave-one-subject-out cross-validation procedure in which a single subject is iteratively left out of the first-stage group analysis. Subsequent analysis is then carried out using the remaining data, and the procedure is then repeated for each subject.

A receiver operating characteristic (ROC curve) analysis was used to determine the best cut-off value that provided the highest sensitivity and specificity. The optimal cut-off values for the ROC analyses were selected depending on the maximum value of the Youden index.

Results:

T2 weighted, T1 weighted post-contrast, FA, MD, AD, RD, CBV and CBF maps from a patient with GII Oligodendroglioma and a patient with GIII Anaplastic Astrocytoma are shown in Figure 2. The median and SD values of these parameters for all GII and GIII gliomas and for sub-group analyses of histological subtypes are shown in Table 1.

On univariate analysis, no significant difference in tumour volume, normalised T2 signal intensity ratio and DSC parameters were observed as shown in Figure 3 ($P > 0.05$). The median FA values were slightly higher in GIII gliomas and the median MD values slightly lower in GIII gliomas; however, there was no significant difference in any DTI parameters as shown in Figure 3 ($P > 0.05$).

The logistic regression analysis showed that the tumour volume and rMTT provided the best combination in separating non-enhancing GII from GIII gliomas. The ROC analysis showed that an optimal cut-off value of 0.33 resulted in 70.6% sensitivity and 64.3% specificity and

an AUC of 0.71 in differentiating GII and GIII gliomas as shown in Figure 4. The "leave-one-out" cross-validation resulted in 67.4% sensitivity and 69.9% specificity to differentiate between GII and GIII gliomas. The ROC analyses of all the parameters are shown in Table 3.

Since oligodendrogliomas are histologically different from astrocytomas, a subgroup analysis was also performed to determine if the imaging parameters were able to differentiate between astrocytomas and oligodendrogliomas. In addition, a sub-analysis was also performed to differentiate between GII and GIII in these histological subtypes. Specifically, differences between GII astrocytoma (n=27) from oligodendroglioma (n=22), GII astrocytoma (n=27) from GIII anaplastic astrocytoma (n=20); and astrocytomas (n=47) from oligodendrogliomas (n=25), were analysed. The results from logistic regression analysis, ROC curve and cross-validation results are shown in Table 4, which clearly demonstrate the utility of different DTI and DSC parameters in separating these histological subtypes with a much higher sensitivity and specificity.

Discussion:

Whilst univariate analysis did not demonstrate significant differences between non-enhancing GII and GIII gliomas, logistic regression analysis suggests that both DTI and DSC imaging may play an important yet complimentary role in predicting the grade of non-enhancing gliomas. When the data was separated between grades as well as histological subtypes of astrocytomas and oligodendrogliomas, the utility of DTI and DSC parameters was more evident (Table 4).

Fractional anisotropy (FA), a quantitative index for water molecular anisotropy [27], provides information about the microstructural organisation of the brain tissue and has been shown to detect microstructural heterogeneity in the brain due to the presence of a tumour. A non-significant but higher FA was observed in GIII non-enhancing gliomas in comparison to GII gliomas in the present study. This is in agreement with previous studies reporting higher FA in HGG relative to LGG [11, 12], but are contrary to the study by Shan, W. et al, (2017), which reported higher FA in LGG [28]. The apparent discrepancy between our findings and this study may be due to the fact that in Shan, W's study all LGG (GI and GII) were compared with HGG (GIII and GIV) which included both enhancing and non-enhancing tumours [28], while in our study, only GII and GIII non-enhancing gliomas were included. The higher FA values observed in GIII gliomas in our study may be due to an increase in the degree of directionality of water diffusion resulting from a decrease in extracellular volume [18], or that the tumour invasiveness (abnormality observed in T2 weighted images used for the VOI)

included some of the normal brain tissue, which may have contributed to increased FA values. The lack of significant differences in FA values in our study may be due to a purely non-enhancing cohort, whereas previous studies have either combined all LGG (G1+GII) and all HGG (GIII+GIV) tumours [3] or included enhancing and non-enhancing gliomas [12].

MD, has been shown to be sensitive to cellularity, oedema, and necrosis [27]. Although one study reported significant differences in MD values between LGG and HGG [9], another study reported no significant difference [3]. Similar to this finding, we observed a lower but non-significant MD_{min} value in GIII, probably reflecting the higher tumour cellularity in GIII gliomas.

The rCBV value serves as an important DSC parameter reflecting tumour haemodynamic properties and has been used for the assessment of tumour vascularity [19]. Previous studies reported that the $rCBV_{max}$ of HGG was significantly higher than LGG [18, 29]. However, another study found no significant difference in rCBV between LGG and HGG [9], similar to our observations. The discrepancies between our findings and previously published papers may be due to the heterogeneity of the tumours included (enhancing versus non-enhancing), the VOI used (we analysed the entire tumour while some previous studies have only focused on the tumour core) [9], or that we included both astrocytomas and oligodendrogliomas, which are two distinct histological subtypes with different sensitivities to chemoradiation therapy. rMTT reflects the time for the contrast bolus to transit through a vessel or tissue of interest [30]. A previous study reported that the MTT values were unable to discriminate between glioma grades [31]. Although we observed similar results when univariate analyses were used, logistic analyses indicated that the tumour volume along with rMTT provided the best combination in separating GII from GIII non-enhancing gliomas. Whilst tumour volume by itself does not reflect tumour biology, the relatively higher tumour volume in GIII gliomas may be due to the fact that more malignant tumours are rapidly proliferating due to the presence of higher hypoxia, which mediates neo-angiogenesis and invasion, which in turn may lead to larger tumours. As the univariate analysis did not demonstrate any significant difference in tumour volume between GII and GIII gliomas, it does not seem to be an independent parameter in the prediction of tumour grade. GIII gliomas demonstrated a lower (faster) rMTT, which may reflect higher vascular permeability due to extended endothelial cell gaps, incomplete basement membrane and lack of pericyte or smooth muscle layering in the higher-grade tumours than GII gliomas. Although the logistic regression analyses demonstrated significant differences, the sensitivity and specificity were modest. A potential reason for the moderate separation may have been due to the fact that it is not just

the malignancy grade (which is defined by mitosis, cell density and necrosis), but also the cell type and vascular structure, as well as the genetic phenotype, that can impact on the tumour growth and its subsequent response to therapy. Inclusion of both astrocytomas and oligodendrogliomas in the GII and GIII tumours in our study, which are histologically different may have masked the differences in the measured parameters.

While comparing distinct histological subtypes, astrocytomas from oligodendrogliomas, we observed that FA and RD provided the best combination to separate these tumour types with much higher sensitivity and specificity and AUC values (Table 4), which may indicate increased myelin disintegration and axonal damage in astrocytomas than oligodendrogliomas. The absence of significant differences in any parameter using univariate analysis may be due to the fact that each group included both GII and GIII tumours, which may have averaged out the differences due to tumour grade.

We therefore did a further analysis within the same grade and compared GII astrocytoma with GII oligodendrogliomas. We observed that higher RD and rCBF in GII astrocytomas provided the best combination to separate these two groups (Table 4). Higher RD is suggestive of myelin disintegration and axonal damage in GII astrocytoma. In addition, lower rCBF in GII oligodendroglioma may be due to the presence of a dense but inefficient network of branching capillaries resembling chicken wire in GII oligodendrogliomas. Similarly, when we compared within the same histological subtype but between different grades (GII astrocytoma versus GIII anaplastic astrocytoma), tumour volume, FA, MD, rCBF and $rCBV_{max}$ provided the best combination in separating between them with an AUC of 0.88, sensitivity of 83.4% and specificity of 62.5 (Table 4). This could be a consequence of rapid tumour growth, increased tumour cellularity, increase in the degree of directionality of water diffusion and increased tumour vascularity in GIII astrocytoma. Though the patient numbers were smaller in the sub-analyses, these results suggest that when a histologically homogenous group of patients are compared, diffusion and perfusion imaging parameters can provide complementary information and help in differentiating non-enhancing gliomas.

Study limitation include a relatively small number of patients within each histological sub-type, (especially for the DTI data). There were only 3 patients with non-enhancing GIII oligodendrogliomas, preventing us from investigating the difference between GII and GIII oligodendrogliomas. Future studies on a larger patient cohort and a prospective study is needed to validate our findings.

Conclusion:

In conclusion, these studies indicate that DTI and DSC-MRI complement standard structural MRI sequences in differentiating between non-enhancing GII and GIII gliomas. Both DTI and DSC-MRI based parameters demonstrated significant added value in differentiating non-enhancing histological subtypes including astrocytomas from oligodendrogliomas, GII astrocytomas from GII oligodendrogliomas and GII astrocytomas from anaplastic (GIII) astrocytomas. However, these studies need to be validated in a larger cohort.

Conflict of interest:

The authors declare no conflict of interest.

References:

1. Kao, H.-W. et al, *Advanced MR imaging of gliomas: an update.* BioMed research international, 2013. p. 970586. DOI: 10.1155/2013/970586.
2. Scott, J. N. et al., *How often are nonenhancing supratentorial gliomas malignant? A population study*. Neurology, 2002. 59(6): p. 947□949. DOI:10.1212/wnl.59.6.947.
3. Liu, X., et al., *MR diffusion tensor and perfusion-weighted imaging in preoperative grading of supratentorial nonenhancing gliomas.* Neuro-oncology, 2011. 13(4): p. 447. DOI: 10.1093/neuonc/noq197.
4. Morita N, et al., *Dynamic susceptibility contrast perfusion weighted imaging in grading of nonenhancing astrocytomas*. J Magn Reson Imaging, 2010. 32(4): p. 803□808. DOI:10.1002/jmri.22324.
5. Forst D.A., et al., *Low-grade gliomas.* Oncologist, 2014. 19(4): p. 403□413. DOI:10.1634/theoncologist.2013-0345.
6. Dixit K, Raizer J. *Newer Strategies for the Management of Low-Grade Gliomas*. Oncology (Williston Park), 2017. 31(9): p680-685. DOI: 29071695.
7. Garcia C.R., et al., *Comprehensive evaluation of treatment and outcomes of low-grade diffuse gliomas. PLoS One*, 2018. 13(9): p. e0203639 DOI:10.1371/journal.pone.0203639.
8. Alkanhal, H., Das, K. and Poptani, H. *Diffusion and perfusion weighted magnetic resonance imaging methods in non-enhancing gliomas*, World Neurosurgery. 2020. DOI: 10.1016/j.wneu.2020.05.278.

9. Fan, G.G., et al., *Usefulness of diffusion/perfusion-weighted MRI in patients with non-enhancing supratentorial brain gliomas: a valuable tool to predict tumour grading?* Br J Radiol, 2006. **79**(944): p. 652-8. DOI: 10.1259/bjr/25349497.
10. Goebell, E., et al., *Low-grade and anaplastic gliomas: differences in architecture evaluated with diffusion-tensor MR imaging.* Radiology, 2006. **239**(1): p. 217-22. DOI: 10.1148/radiol.2383050059.
11. Lee, H.Y., et al., *Diffusion-tensor imaging for glioma grading at 3-T magnetic resonance imaging: analysis of fractional anisotropy and mean diffusivity*. Journal of computer assisted tomography, 2008. **32**(2): p. 298-303. DOI:10.1097/RCT.0b013e318076b44d.
12. Inoue, T., et al., *Diffusion tensor imaging for preoperative evaluation of tumor grade in gliomas.* Clin Neurol Neurosurg, 2005. **107**(3): p. 174-80. DOI: 10.1016/j.clineuro.2004.06.011.
13. Beppu, T., et al., *Measurement of fractional anisotropy using diffusion tensor MRI in supratentorial astrocytic tumors.* J Neurooncol, 2003. **63**(2): p. 109-16. DOI: 10.1023/a:1023977520909.
14. Saini, J., et al., *Comparative evaluation of cerebral gliomas using rCBV measurements during sequential acquisition of T1-perfusion and T2*-perfusion MRI*. 2019. 14(4): p. e0215400. DOI: 10.1371/journal.pone.0215400.
15. Xu, W., et al., *The performance of MR perfusion-weighted imaging for the differentiation of high-grade glioma from primary central nervous system lymphoma: A systematic review and meta-analysis.* PLoS One, 2017. **12**(3): p. e0173430. DOI: 10.1371/journal.pone.0173430.

16. Duc, N.M., et al., *Clinical approach of perfusion-weighted imaging.* Imaging in Medicine, 2018. **10**(3): p. 69-78.
17. Barajas, R.F., Jr. and S. Cha, *Benefits of dynamic susceptibility-weighted contrast-enhanced perfusion MRI for glioma diagnosis and therapy.* CNS Oncol, 2014. **3**(6): p. 407-19. DOI: 10.2217/cns.14.44.
18. Sahin, N., et al., *Advanced MR Imaging Techniques in the Evaluation of Nonenhancing Gliomas: Perfusion-Weighted Imaging Compared with Proton Magnetic Resonance Spectroscopy and Tumor Grade.* Neuroradiology Journal, 2013. **26**(5): p. 531-541. DOI: 10.1177/197140091302600506.
19. Maia, A.C., Jr., et al., *MR cerebral blood volume maps correlated with vascular endothelial growth factor expression and tumor grade in nonenhancing gliomas.* AJNR Am J Neuroradiol, 2005. **26**(4): p. 777-83. PMID: 15814920.
20. Geneidi, E.A.S.H., et al., *Potential role of quantitative MRI assessment in differentiating high from low-grade gliomas.* The Egyptian Journal of Radiology and Nuclear Medicine, 2016. **47**(1): p. 243-253. DOI: 10.1016/j.ejrnm.2015.11.005.
21. Khalid, L., et al., *Imaging characteristics of oligodendrogliomas that predict grade.* AJNR Am J Neuroradiol, 2012. **33**(5): p. 852-7. DOI: 10.3174/ajnr.A2895.
22. Saito, T., et al., *Role of perfusion-weighted imaging at 3T in the histopathological differentiation between astrocytic and oligodendroglial tumors.* Eur J Radiol, 2012. **81**(8): p. 1863-9 DOI: 10.1016/j.ejrad.2011.04.009.
23. Bjornerud, A., et al., *T1- and T2*-dominant extravasation correction in DSC-MRI: part I--theoretical considerations and implications for assessment of tumor hemodynamic*

properties. J Cereb Blood Flow Metab, 2011. **31**(10): p. 2041-53. DOI: 10.1038/jcbfm.2011.52.

24. Chen, S., et al., *Automated Determination of Arterial Input Function for Dynamic Susceptibility Contrast MRI from Regions around Arteries Using Independent Component Analysis.* Radiol Res Pract, 2016. **2016**: p. 2657405. DOI: 10.1155/2016/2657405.
25. Østergaard, L., et al., *High resolution measurement of cerebral blood flow using intravascular tracer bolus passages. Part I: Mathematical approach and statistical analysis.* Magnetic resonance in medicine, 1996. **36**(5): p. 715-725. DOI: 10.1002/mrm.1910360510.
26. Andersson, J.L.R. and S.N. Sotiropoulos, *An integrated approach to correction for off-resonance effects and subject movement in diffusion MR imaging.* Neuroimage, 2016. **125**: p. 1063-1078. DOI: 10.1016/j.neuroimage.2015.10.019.
27. Server, A., et al., *Analysis of diffusion tensor imaging metrics for gliomas grading at 3 T.* Eur J Radiol, 2014. **83**(3): p. e156-65 DOI: 10.1016/j.ejrad.2013.12.023.
28. Shan, W., Wang, X., *Clinical application value of 3.0T MR diffusion tensor imaging in grade diagnosis of gliomas*. Oncology Letters, 2017. **14**(2): p. 2009-2014 DOI:10.3892/ol.2017.6378
29. Law, M., et al., *Glioma grading: sensitivity, specificity, and predictive values of perfusion MR imaging and proton MR spectroscopic imaging compared with conventional MR imaging.* AJNR Am J Neuroradiol, 2003. **24**(10): p. 1989-98.

30. Pizzolato, M., T. Boutelier, and R. Deriche, *Perfusion deconvolution in DSC-MRI with dispersion-compliant bases.* Med Image Anal, 2017. **36**: p. 197-215 DOI: 10.1016/j.media.2016.12.001.

31. Law, M., et al., *Comparing perfusion metrics obtained from a single compartment versus pharmacokinetic modeling methods using dynamic susceptibility contrast-enhanced perfusion MR imaging with glioma grade.* American journal of neuroradiology, 2006. **27**(9): p. 1975-1982.

Figure Legends:

Figure 1: Left, original T2, FA and CBV images (A) and after resampling to match the resolution of CBV maps (B). Right, representative tumour VOI (blue) overlaid on a resampled T2 image that was used to analyse the tumour data.

Figure 2: T2 weighted images from a patient with a non-enhancing GII oligodendroglioma (A) and an anaplastic astrocytoma GIII (B). The tumour appears hyper-intense on T2 weighted images. In A, the tumour is located in the left temporal lobe, while in B the hyperintense lesion on T2 is centred within the left insular cortex. Post-contrast T1 weighted images, CBV and CBF maps show the location of the tumour (blue arrows). Corresponding FA, MD, AD and RD maps from both the patients are shown in the lower rows.

Figure 3: Box plots of tumour volume (A, cm^3), normalised T2 signal intensity (B, SI), $rCBV_{max}$ (C), rCBF (D), FA (E), MD_{min} (F, $\times 10^{-3}$ mm^2/s), AD (G, $\times 10^{-3}$ mm^2/s), RD (H $\times 10^{-3}$ mm^2/s) from GII and GIII gliomas. The bottom and top lines of the box demarcate the 25th and 75th percentile respectively, while the line inside the box is the median, (▪) is the mean and (*) denotes outliers. The whiskers show the 5th and 95th percentile

Figure 4: ROC curves for GII and GIII non enhancing gliomas.

Table 2: Median and standard deviation values of tumour volume (TV, cm^3), normalised T2 signal intensity ratio, DTI and DSC parameters for GII and GIII gliomas and for sub-group analysis.

Parameters	GII	GIII	GII A	GII OD	GIII AA	GIII AO
TV	16.71±22.62	25.55±23.56	14.84±25.58	17.54±18.92	30.45±24.45	18.72±9.81
nT2	1.64±0.43	1.62±0.41	1.58±0.38	1.77±0.47	1.67±0.41	1.36±0.10
FA	0.10± 0.04	0.12±0.05	0.10± 0.04	0.10±0.03	0.11±0.06	0.15±0.00
MD_{min}	1.0±2.5	1.1±2	1.0±3.2	1.1±1.8	1.1±2	0.8±0.1
AD	1.0±0.25	1.5±0.35	1.6±0.28	1.5±0.21	1.7±0.33	1.1±0.22
RD	1.0±0.28	1.2±0.35	1.3±0.32	1.2±0.21	1.4±0.34	0.9±0.1
$rCBV_{max}$	2.11± 0.92	2.12± 0.95	1.92± 0.91	2.32±0.95	2.04±0.86	2.17 ± 0.45
rCBF	0.94± 0.42	1.09± 1.88	1.08±0.72	0.92±0.69	1.04±1.96	1.66 ± 1.27
rMTT	0.91± 0.51	0.85± 0.38	1.02±0.5	0.91±0.53	0.88±0.39	0.55 ± 0.19

A=Astrocytoma, OD= Oligodendroglioma, AA= Anaplastic Astrocytoma and AO= Anaplastic Oligodendroglioma, nT2 = normalised T2 signal intensity ratio, MD_{min}, AD and RD values ($\times 10^{-3}$ mm^2/s)

Table 3: ROC curve analysis for the parameters analysed to differentiate between GII and GIII non-enhancing glioma. Cut-off values, specificity and sensitivity were selected based on the maximum value of Youden index.

GII versus GIII					
Parameter	Cut-off	Sensitivity %	Specificity %	AUC	CI
TV + rMTT	0.33	70.60	64.30	0.71	0.55 – 0.86
nT2	1.69	41.20	64.30	0.48	0.30 – 0.66
$rCBV_{max}$	1.79	82.40	50.00	0.53	0.36 – 0.71
rCBF	1.49	35.30	82.10	0.53	0.35 –0.71
FA	0.11	64.70	67.90	0.61	0.44 – 0.79
MD_{min}	1.00	76.50	32.10	0.47	0.30 – 0.64
AD	1.61	47.10	64.30	0.47	0.29 – 0.66
RD	1.31	47.10	64.30	0.45	0.27 – 0.63

AUC: Area under the Curve and CI: confidence interval. MD_{min}, AD and RD values ($\times 10^{-3}$ mm^2/s)

Table 4: Summary results from logistic regression analysis, ROC curve and "leave-one-out" cross-validation for the subgroup.

Group	LRA parameters	ROC curve Results			LOOCV results	
		Sensitivity %	Specificity %	AUC	Sensitivity %	Specificity %
GII Astocyotma vs Oligodendroglioma	nT2, RD & rCBF	85%	64.3%	0.78	64.2	93.1
GII vs GIII Astrocytoma	TV, FA, MD_{min} & rCBF	68.8%	92.9%	0.88	83.4	62.5
Astrocytoma vs Oligodendroglioma	FA & RD	87.5%	50%	0.69	82.6	32.7

AUC: Area under the Curve, LRA: Logistic regression analysis, TV: Tumour volume, LOOCV: Leave-one-out cross validation.

Table 1: Summary of the number of patients, grade and pathology

Grade	Pathology	Number of patients	Total
Grade II	Astrocytoma	27	49
	Oligodendroglioma	22	
Grade III	Anaplastic Astrocytoma	20	23
	Anaplastic Oligodendroglioma	3	

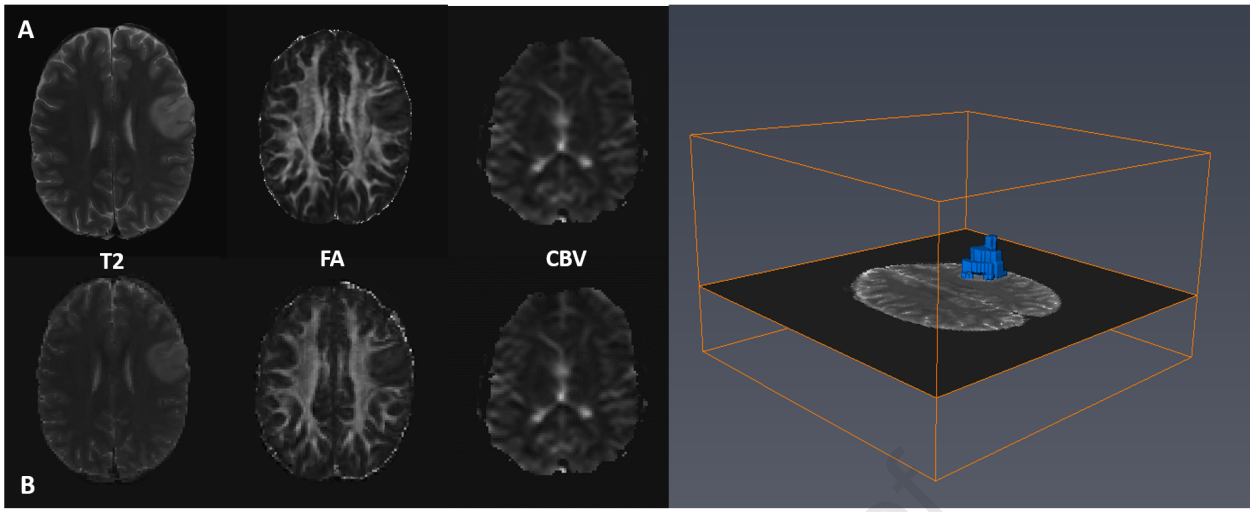

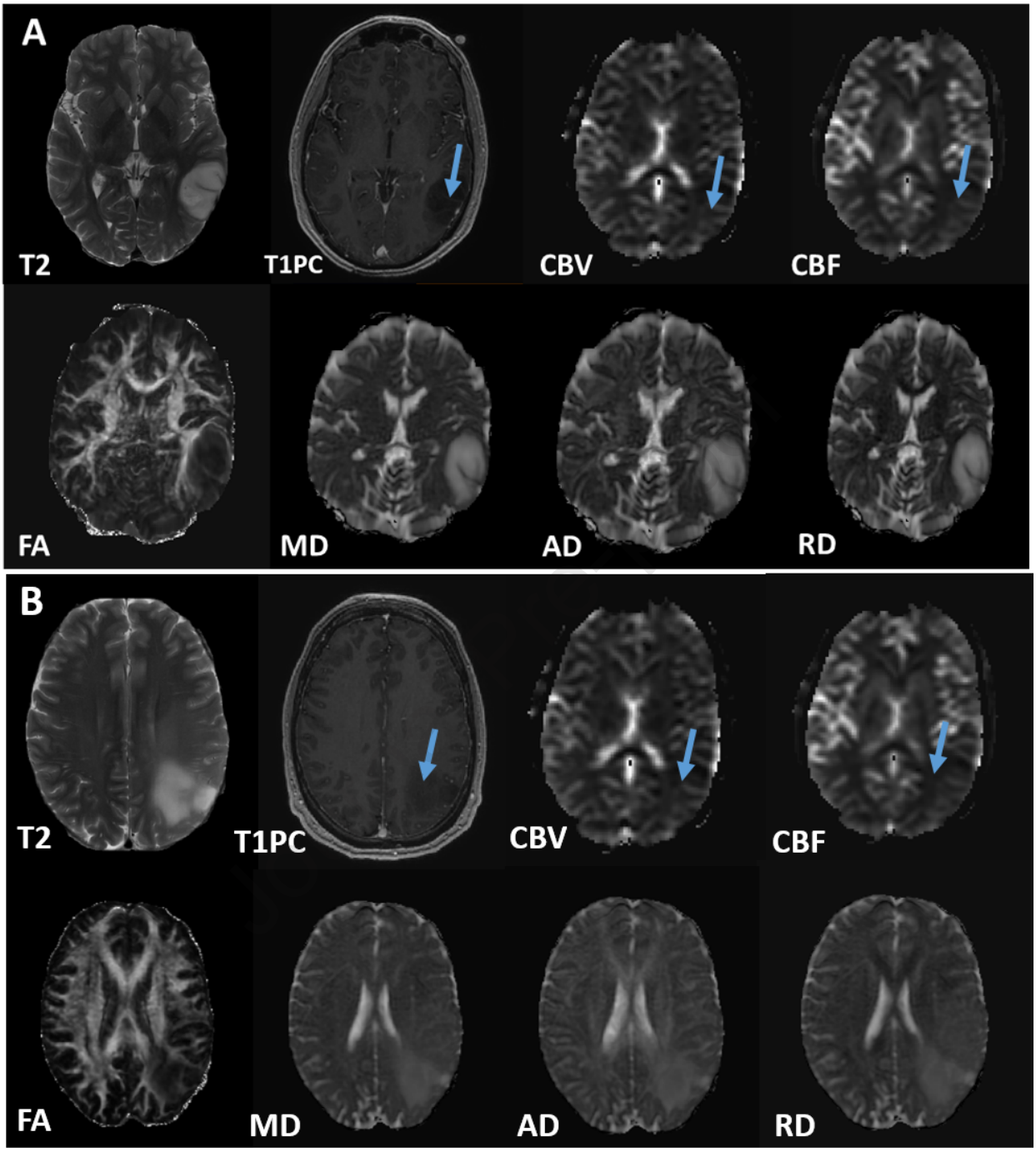
A
T2
T1PC
CBV
CBF
FA
MD
AD
RD
B
T2
T1PC
CBV
CBF
FA
MD
AD
RD

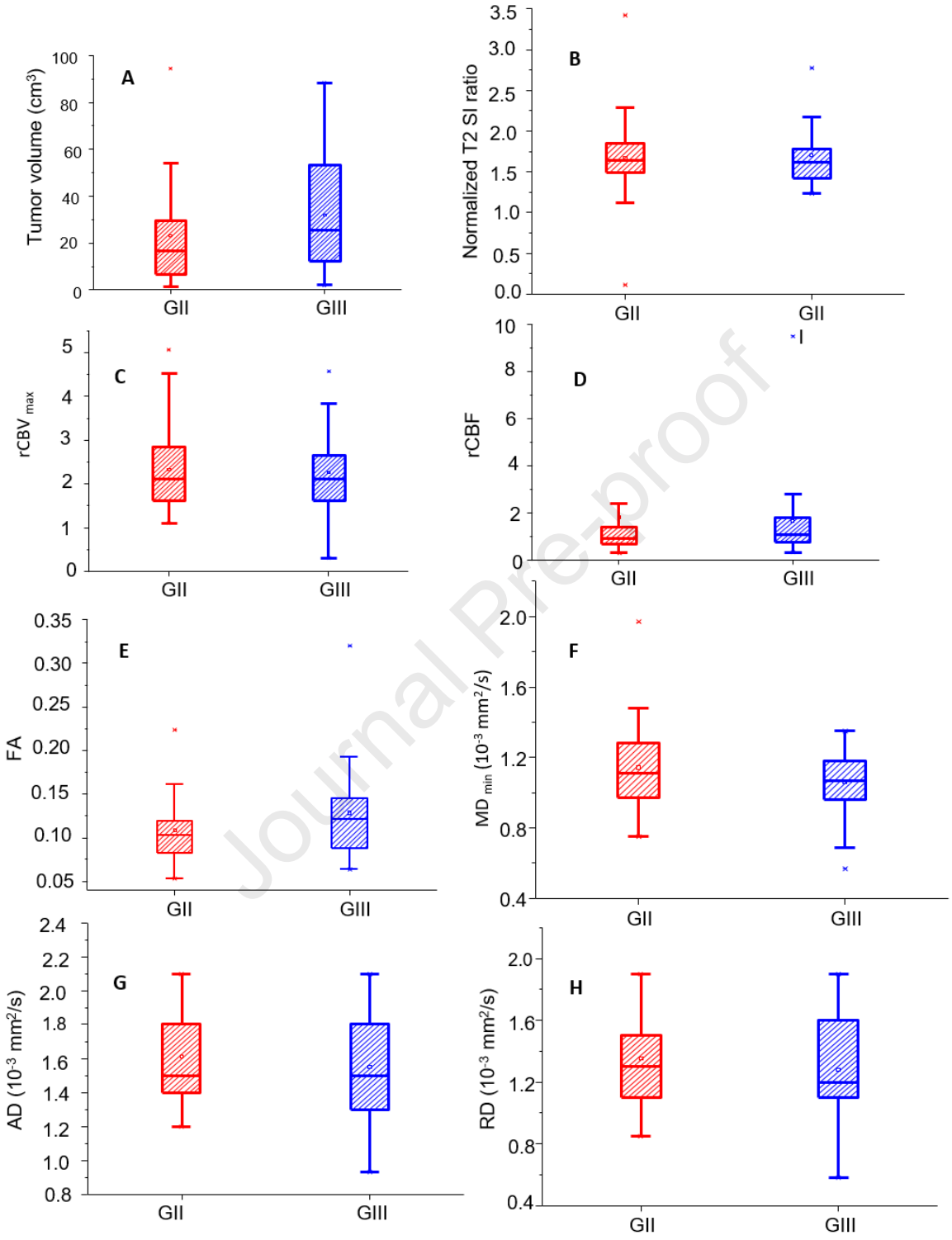

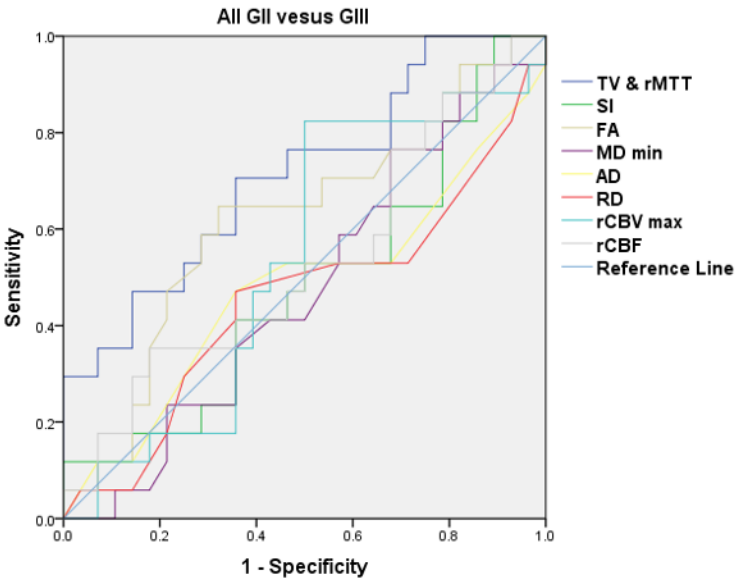

Conflict of interest:

The authors declare no conflict of interest with regards to the work submitted

Abbreviation List:

ADC = Apparent Diffusion Coefficient

AUC = Area under the Curve

AD = Axial Diffusivity

AIF = Arterial Input Function

CNS = Central Nervous System.

CBF = Cerebral Blood Flow

CBV = Cerebral Blood Volume

CI = Confidence Interval

DTI = Diffusion Tensor Imaging

DSC = Dynamic-Susceptibility Contrast

FA = Fractional Anisotropy

FMRIB = Functional Magnetic Resonance Imaging of Brain

HGG = High-grade Glioma

LGG = Low-Grade Glioma

LRA = Logistic Regression Analysis

LOOCV = Leave-One-Out Cross Validation

MD = Mean Diffusivity

MTT = Mean Transit Time

MRI = Magnetic Resonance Imaging

PWI = Perfusion Weighted Imaging

r = relative

RD = Radial Diffusivity

ROC = Receiver Operating Characteristic

sSVD = standard Singular Value Decomposition

TV = Tumor Volume

VOI = Volume Of Interest

WHO = World Health Organization